Construction and Building Materials 313 (2021) 125413

Contents lists available at ScienceDirect

Construction and Building Materials

journal homepage: www.elsevier.com/locate/conbuildmat

Application of Fourier Transform infrared spectroscopy (FTIR) coupled with multivariate regression for calcium carbonate ($CaCO_3$) quantification in cement

Victor Hugo Jacks Mendes dos Santos [a,b], Darlan Pontin [a], Gabriela Gonçalves Dias Ponzi [a,b], Amanda Sofia de Guimarães e Stepanha [a,b], Renan Bordulis Martel [a], Marta Kerber Schütz [a,c], Sandra Mara Oliveira Einloft [a,b,c], Felipe Dalla Vecchia [a,b,c,*]

[a] Pontifical Catholic University of Rio Grande do Sul, PUCRS. Institute of Petroleum and Natural Resources, Avenida Ipiranga, 6681, – TECNOPUC, Building 96J, 90619-900, Porto Alegre, Brazil
[b] Pontifical Catholic University of Rio Grande do Sul, PUCRS, Graduate Program in Materials Engineering and Technology, Avenida Ipiranga, 6681– Building 32, 90619-900, Porto Alegre, Brazil
[c] Pontifical Catholic University of Rio Grande do Sul, PUCRS, School of Technology, Avenida Ipiranga, 6681 – Building 30, 90619-900, Porto Alegre, Brazil

ARTICLE INFO

Keywords:
Accelerated carbonation
Carbon capture and storage
Natural carbonation
Carbonation curing
Chemometrics
Multivariate analysis

ABSTRACT

Partial least squares (PLS) regression models were developed to quantify $CaCO_3$ in cement and to study the CO_2 effect on the material matrix. PLS results presented good correlation coefficient (R^2 = 0.9995) and low estimation error (RMSEP = 3.61 mg $CaCO_3$/g cement). From the results, it was observed that the portlandite consumption, the increase in $CaCO_3$ content and the C-S-H decalcification-polymerization are the most relevant cement chemical transformations. Thus, it was concluded that: *i*) it is possible to obtain fast, low-cost, and reliable models to quantify $CaCO_3$ by FTIR and *ii*) the method is applicable to study carbonated cement-based materials.

1. Introduction

Greenhouse gases (GHG) influence on the environment is one of the humanity's greatest concerns in the 21st century. Emissions of greenhouse gases, such as methane (CH_4) and carbon dioxide (CO_2), are among the main drivers of global warming [1–3]. Currently, the main sources of GHG emissions are related to: (*i*) energy from fossil fuels, (*ii*) land use change and deforestation and (*iii*) decomposition of minerals (carbonates) [1,4–5]. In this context, the largest emission source from carbonate decomposition comes from cement production chain, representing about 5 to 7% of the global emissions budget [6–7].

Cement is one of the most important materials in civil construction and is applied as a binding agent in structural foundations or as a protective element [8]. Within this context, cement and CO_2 are two topics of interest to the academic community and are often closely related. Although the environmental issue is predominant, with attention focused on mitigating the impacts associated with the cement production chain, there are key issues under discussion about the influence of CO_2 on the performance or integrity of cementitious materials. All cement-based material undergoes a certain level of carbonation throughout its life cycle due to its chemical composition [9–10]. Thus, carbonation is a topic of great interest in several economic segments [10–11]. While the research topics: (*i*) natural carbonation (atmospheric carbonation), (*ii*) accelerated carbonation and (*iii*) well cement carbonation, focus on material integrity issues [6,12–15], the fields of study: (*iv*) carbonation curing (accelerated curing) and (*v*) CO_2 mineralization (mineral sequestration), evaluate cement-based materials in the context of Carbon Capture, Utilization, and Storage (CCUS) [13,16–17].

Portland cement is a dominant class of cementitious materials. It is composed of four main compounds: tricalcium silicate (C_3S - Ca_3SiO_5 - alite), dicalcium silicate (C_2S - Ca_2SiO_4 - belite), tricalcium aluminate (C_3A - $Ca_3Al_2O_6$ - celite) and tetracalcium aluminoferrates (C_4AF - $Ca_4Al_2Fe_2O_{10}$ - brownmillerite) [18–21]. These compounds are hydrated during the cement curing process, that takes place over several days and gives the necessary mechanical and chemical characteristics to the

* Corresponding author at: Pontifical Catholic University of Rio Grande do Sul, PUCRS. Institute of Petroleum and Natural Resources, Avenida Ipiranga, 6681, – TECNOPUC, Building 96J, 90619-900, Porto Alegre, Brazil.
E-mail addresses: victor.santos@pucrs.br (V.H.J.M. Santos), felipe.vecchia@pucrs.br (F. Dalla Vecchia).

https://doi.org/10.1016/j.conbuildmat.2021.125413
Received 18 June 2021; Received in revised form 4 October 2021; Accepted 25 October 2021
Available online 12 November 2021

material for several application [18,22–25]. The main hydration products are calcium silicate hydrate (C-S-H), a semi-amorphous phase responsible for the cement mechanical properties, and portlandite [CH - calcium hydroxide - $Ca(OH)_2$], which serves as an alkaline reserve of the material and is characterized by having a crystalline structure [19,26–28].

The main components of cementitious materials are sensitive to the CO_2 action and are subject to the carbonation process [3,29]. These chemical processes produce calcium carbonate ($CaCO_3$) and amorphous silica, among other minority compounds, which induce several changes in the chemical composition, mechanical strength, and pore size distribution of the cement matrix [30]. The main consequence of CO_2 attack on the cement matrix is a potential loss of material's integrity [27], which can be accelerated by exposure to supercritical CO_2 [31]. In this context, some factors can influence the carbonation rate of cement, including: (*i*) curing conditions of the material, (*ii*) type of cement (chemical composition), (*iii*) presence of additives and (*iv*) water-to-cement ratio [65]. Thus, it is of great importance to develop methods that can be used to evaluate the extent of the carbonation process of cementitious materials.

Because of the complexity of cementitious materials, it is necessary to employ several complementary analytical techniques to comprehensively characterize such materials [32–33]. Furthermore, when the carbonation process is considered, many difficulties and uncertainties are added to research and development projects [34]. In this context, it is essential to: (*i*) quantify the carbonation reaction products, (*ii*) control the carbonation process and (*iii*) understand its effects on the cement integrity and properties. Thus, techniques such as phenolphthalein test, X-ray florescence (XRF), X-ray diffraction (XRD), transmission electron microscopy (TEM), scanning electron microscopy (SEM), X-ray microtomography (MicroCT), thermogravimetric analysis (TGA), nuclear magnetic resonance (NMR) spectroscopy and infrared (IR) spectroscopy are widely applied in the literature to characterize carbonated cementitious materials and their composites [32,35–38]. Among the characterization methods, the analysis of $CaCO_3$ in cementitious materials can be performed in the following way: (*i*) qualitative, by means of phenolphthalein, TEM and SEM methods, (*ii*) semi-quantitative, using the IR, MicroCT, XRD and XRF instruments and (*iii*) quantitative, through TGA analysis [11,35–36,39–40]. In addition, XRD, SEM, IR and TGA can be applied, with their respective limitations, to identify the presence of different $CaCO_3$ polymorphs (amorphous carbonate, vaterite, aragonite and calcite) [31,41–42]. Otherwise, NMR is applied only to analyze the siliceous (^{29}Si NMR) and aluminate (^{27}Al NMR) cement phases; however, it is not usually applied to analyze $CaCO_3$ from ^{13}C NMR [11,39,43].

The quantitative analysis of $CaCO_3$ in the cementitious matrix is one of the central points in all studies involving the carbonation process. However, the characterization methods suffer from one or more restrictions related to: (*i*) equipment availability, (*ii*) sensitivity and specificity of the method, (*iii*) lack of specialized human resources, (*iv*) analysis cost and/or (*v*) time-consuming procedures for sample preparation and analysis [38,40,44]. Thus, developing new solutions that allow fast, low-cost, and reliable quantification of $CaCO_3$ content in cementitious matrix is necessary. In this context, it was identified that Fourier Transform Infrared Spectroscopy (FTIR) is a technique that meets all the listed requirements. FTIR is widely available in analysis laboratories, is simple and easy to operate, performs fast and non-destructive analysis, requires small amounts of sample (0.1 g), presents few sample preparation steps, is versatile and capable of evaluating both amorphous and crystalline matrices, presents low operation and maintenance cost, and generates substantial amounts of data (spectra) [8,39,45–49]. In the study of cement-based materials, FTIR is normally applied as a complementary analytical tool to evaluate hydration or carbonation products at qualitative or semi-quantitative level [8–9,39,46]. However, for quantitative purposes, FTIR could be coupled with multivariate analysis (MVA) to increase the sensitivity and specificity of the method.

Previously, FTIR was applied for quantitative analysis of $CaCO_3$ in: (*i*) carbonate rock [40], (*ii*) diatomite ore [50], (*iii*) sediments [45,49,51–53], (*iv*) soil [54] and (*v*) cement [55–56]. Among the studies involving the $CaCO_3$ quantification in cement, it was observed that Hughes et al. [56] applied the Diffuse Reflectance Mid-Infrared Fourier Transform Spectroscopy (DRIFTS) coupled with multivariate analysis to estimate the $CaCO_3$ content in API well cements with known elemental composition and varied origin. However, despite presenting partial least squares (PLS) regression with a good correlation coefficient (R^2 = 0.9950), the model's application range was limited to 0 to 2 wt.% of $CaCO_3$. On the other hand, Legodi et al. [55] applied the FTIR to calibrate a quantitative model to estimate the $CaCO_3$ content in limestone and neat cement mixtures, covering the range of 0 to 100% by weight. The best model was obtained from the integrated area of the carbonate peak (CO_3^{2-}) at 876 cm^{-1} presenting a good correlation coefficient (R^2 = 0.9990). However, none of these studies considered the effect of the carbonation reaction on the cement. Thus, it was not possible to assess whether there is a matrix effect resulting from other products of the carbonation reaction as well as the influence of these transformations in the FTIR spectrum and in the predictive capacity of quantitative models. In addition, both works applied KBr to perform sample preparation [55–56], which adds an additional analysis procedure step and a new source of possible measurement errors. To our knowledge, since Legodi et al. [55], there was no research proposing methods to quantify $CaCO_3$ in cement by FTIR.

In this context, it was proposed in this work to use the Fourier Transform Infrared Spectroscopy (FTIR) and multivariate calibration as a fast, low-cost, and reliable solution to obtain quantitative models to analyze $CaCO_3$ content in cement. The analyzes were performed using the Attenuated Total Reflectance (ATR) accessory, which requires a reduced number of preparation steps [32,40]. API class G cement was used as reference and the material was submitted to carbonation process with supercritical CO_2. Previously, no study considered the effect of the carbonation reaction on the cement matrix to develop quantitative models. It should be emphasized that carbonation reaction influence on the cement properties (chemical and physical). Thus, it is necessary to study the effect of chemical transformations resulting from the exposure of cement to supercritical CO_2 on the quality of predictive models. In this way, the multivariate calibration model was developed with a carbonated cementitious material. It is noteworthy that the application of CO_2 curing and/or CO_2 mineralization (mineral sequestration) to mitigate environmental impacts is beyond the scope of this study.

2. Materials and methods

2.1. Materials

Calcium oxide (Êxodo, 95%), calcium carbonate (calcite $CaCO_3$, Merck – 99.9%), phosphoric acid (Sigma-Aldrich, 85%), carbon dioxide – CO_2 (Air Products, 99.99%) and phenolphthalein (Química Moderna, analytical grade) were used without further purification and its basic properties are detailed in Table S1 (Supplementary Material). The cement applied in this study was an API class G cement (Lafarge Holcim)

Table 1
Chemical composition of API Class G cement.

Chemical composition	Percentage [%]
SiO_2	29.25
Al_2O_3	3.95
Fe_2O_3	4.57
CaO	65.07
MgO	2.32
SO_3	2.27
Na_2O	0.25
K_2O	0.33

and its chemical composition is shown in Table 1.

2.2. Sample preparation

Class G cement paste (cement anhydrous + water) was prepared following the recommendations of American Petroleum Institute specification 10A [57]. The cement paste was prepared with no additives using 0.44 water-to-cement ratio. The detailed procedure for preparing the cement paste using a Chandler Engineering mixer (model 3260) is: (*i*) initially, water is added to the mixing vessel, (*ii*) the cement powder is added over a 15 s mixing cycle at 4,000 rpm and (*iii*) the final mixing is carried out through a second mixing cycle of 35 s at 12,000 rpm. Then, the cement paste is poured into 16 PVC molds (Figure S1 - Supplementary Material), the molds are closed and cured in a thermostatic bath at 65 °C and at atmospheric pressure for 14 days. After curing, cylindrical cement specimens were demolded, and their dimensions were adjusted to 22 mm in diameter and 44 mm in height with a low-speed cutter (Isomet).

2.2.1. Preparation of non-carbonated cement powder

Cured cement specimens were ground in a ball mill (De Leo 0907) to obtain the non-carbonated cement powder (C1 - non-carbonated). Half (8) of the class G cement specimens were ground in a cylindrical vessel (17.8 cm in height and 17.8 cm in diameter) under 150 rpm for 12 h, while the other half (8) were used to study the carbonation process of cylindrical cement specimens. The load of the grinding steel balls was: Ø50 mm balls (5 units), Ø40 mm balls (5 units), Ø32 mm balls (5 units), Ø15 mm balls (5 units), Ø25 mm balls (24 units), Ø19 mm balls (15 units) and Ø10 mm balls (21 units). After grinding, the cement powder was manually sieved through #270 mesh sieve and stored in a desiccator.

2.3. Carbonation with supercritical CO_2

Cement carbonation experiments (cylindrical specimens and powders) were conducted in an HPHT (high pressure-high temperature) pressure vessel under CO_2 supercritical environment, as shown in Fig. 1. The supercritical state is a special condition in which fluids acquire unique properties, being reached by CO_2 at pressures greater than 7.39 MPa and temperatures above 31.1 °C [30,58]. Eight cylindrical cement specimens were exposed to a supercritical CO_2-ultrapure water system at 65 °C and 15 MPa for 7 days (wet carbonation). Such reaction conditions simulate environments compatible with the application of cement in Carbon Capture and Storage (CCS) wells. The quasi-static reaction environment is reported as the most appropriate model to simulate the well dynamics [22,59], since continuous and extensive failures are not frequent in geological formations [60]. The experiment with cylindrical specimens was carried out to evaluate the behavior of the cement material when exposed to supercritical CO_2. After the carbonation experiments, the cylindrical cement specimens were evaluated by the phenolphthalein test, SEM-EDS microscopy and MicroCT analysis.

The experiment with the cement powder was carried out to accelerate the carbonation processes from the exposure of the material to supercritical CO_2 [31]. C1 sample (non-carbonated cement) was exposed to a supercritical CO_2-ultrapure water system at 65 °C and 15 MPa for 7 days. After the reaction with CO_2, both solid and liquid fractions from the HPHT pressure vessel were dried together in an oven at 60 °C for 24 h, obtaining a homogeneous solid fraction with a whitish color. After the carbonation experiments, the non-carbonated (C1) and carbonated (C11) cement powders were evaluated by the XRD diffraction, SEM-EDS microscopy, gas chromatography analysis and FTIR spectroscopy.

2.3.1. Cement carbonation reactions

In the present work, the carbonation process in an aqueous medium

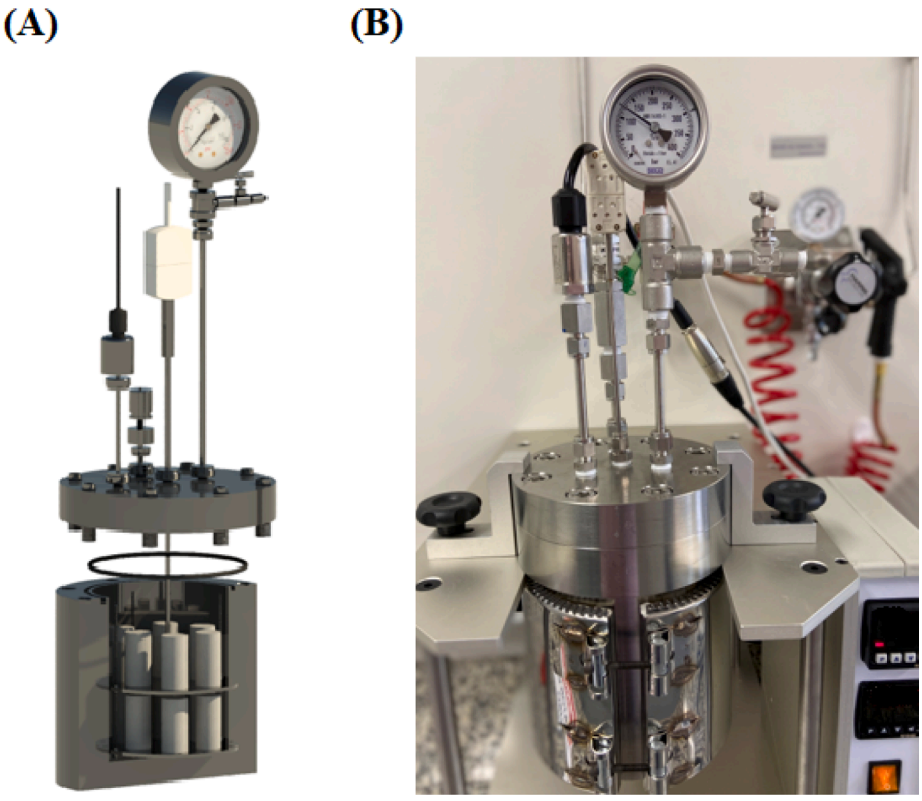

Fig. 1. Experimental arrangement to perform cement specimen's carbonation experiments with supercritical CO_2: (A) conceptual design and (B) high pressure-high temperature (HPHT) pressure vessel.

(wet carbonation) was carried out to simulate the conditions of CCS reservoirs. Based on the literature, the main carbonation reactions consume the calcium silicate hydrate (C-S-H) and portlandite (CH) phases, producing different calcium carbonate ($CaCO_3$) polymorphs (amorphous, calcite, aragonite and vaterite) and amorphous silica [24,61]. In addition, non-hydrated cement fractions (C_3S and C_2S) are also consumed by the carbonation process and produce $CaCO_3$ and siliceous products. These reactions are represented by Equations 1–8 [12–13,22].

$$C_3S_{(s)} + 3CO_{2(aq)} + nH_2O_{(l)} \rightarrow SiO_2.nH_2O_{(s)} + 3CaCO_{3(s)} \quad (1)$$

$$C_2S_{(s)} + 3CO_{2(aq)} + nH_2O_{(l)} \rightarrow SiO_2.nH_2O_{(s)} + 3CaCO_{3(s)} \quad (2)$$

$$Ca(OH)_{2(s)} + CO^{2-}_{3(aq)} + 2H^{+}_{(aq)} \rightarrow CaCO_{3(s)} + 2H_2O_{(l)} \quad (3)$$

$$Ca(OH)_{2(s)} + HCO^{-}_{3(aq)} + H^{+}_{(aq)} \rightarrow CaCO_{3(s)} + 2H_2O_{(l)} \quad (4)$$

$$C-S-H_{(s)} + CO^{2-}_{3(aq)} + 2H^{+}_{(aq)} \rightarrow CaCO_{3(s)} + SiO_xOH_{x(s)} \quad (5)$$

$$C-S-H_{(s)} + HCO^{-}_{3(aq)} + H^{+}_{(aq)} \rightarrow CaCO_{3(s)} + SiO_xOH_{x(s)} \quad (6)$$

$$CaCO_{3(s)} + CO_{2(g)} + H_2O_{(l)} \leftrightarrow Ca^{2+}_{(aq)} + HCO^{-}_{3(aq)} \quad (7)$$

$$CaCO_{3(s)} + 2H^{+}_{(aq)} \leftrightarrow CO_{2(g)} + H_2O_{(l)} + Ca^{2+}_{(aq)} \quad (8)$$

2.4. Sample characterization

In the present work, the following characterizations methods were performed to analyze the non-carbonated and carbonated cement samples: (*i*) phenolphthalein test, (*ii*) X-ray microtomography analysis (MicroCT), (*iii*) scanning electron microscopy (SEM), (*iv*) X-ray diffraction analysis (XRD), (*v*) gas chromatography to estimate carbonation degree of cement powder, and (*iv*) Fourier Transform Infrared Spectroscopy (FTIR). The experimental procedures and analytical methods are detailed below.

2.4.1. Phenolphthalein test

The phenolphthalein test is one of the most used methods to evaluate the carbonation of cementitious materials [9,62]. In this test, the cylindrical cement specimens were cut longitudinally, and a solution of phenolphthalein (2%) in ethyl alcohol-water (48:50 v%) was sprayed on the surface of the material to highlight the boundaries of non-carbonated (pink colored) and carbonated (grey colored) cement phases.

2.4.2. X-ray microtomography analysis (MicroCT)

X-ray microtomography (MicroCT) analysis was performed on the Skyscan 1173 X-Ray Microtomograph (Bruker) following the manufacturer's recommendations. The cylindrical cement specimens were analyzed by MicroCT before and after the carbonation process to evaluate the effect of supercritical CO_2 on the microstructure of the material using a non-destructive method.

2.4.3. Scanning electron microscopy (SEM)

The analysis of cement by scanning electron microscopy with energy dispersive X-ray spectroscopy (SEM-EDS) was performed using the Inspect F50 - FEI microscope to: (*i*) characterize the structure of the cement, (*ii*) analyze the elementary profile of cement specimens after the carbonation process (elemental mapping) and (*iii*) characterize the morphological structure of the cement powder before and after the carbonation process.

2.4.4. X-ray diffraction analysis (XRD)

Mineral composition analyzes were performed using an XRD diffractometer D8 Advance A25 (Bruker) at a voltage of 40 kV, a current of 30 mA with Cu-Kα radiation and a scanning step size 0.02° in the θ-2θ ranging from 2 to 80°. The mineral composition of the cement powder was analyzed by XRD before and after the carbonation process.

2.4.5. Carbonation degree of cement powder

Before developing the $CaCO_3$ quantification method in cement by FTIR, it was necessary to estimate the $CaCO_3$ content of the samples in an appropriate unit of measurement. In the present work, mg $CaCO_3$/g cement was proposed as the appropriate unit of measurement. A detailed description of the sample preparation, characterization procedures and the results of analysis are presented in the Supplementary Material (Table S2 and Figure S2) [9,63–64]. Thus, the calcium carbonate content of the non-carbonated (C1 – 45.80 mg $CaCO_3$/g cement) and carbonated (C11 – 468.20 mg $CaCO_3$/g cement) samples were estimated from the experimental analysis, while the carbonation degree of the non-carbonated (C1 – 3.80%) and carbonated (C11 – 38.82%) samples were estimated from Equation (9) and (10).

$$Max\,CO_2\,uptake\,(\%) = 0.785(CaO - 0.7SO_3) + 1.091MgO + 1.420Na_2O + 0.935K_2O \quad (9)$$

$$Carbonation\ degree\ (\%) = 100x\frac{CO_2\ uptake}{max\ CO_2\ uptake} \quad (10)$$

From the results, it was observed that the non-carbonated cement powder (C1) underwent a partial process of natural carbonation, while the carbonated cement powder (C11) was considerably transformed from the reaction with supercritical CO_2. Thus, this information is essential for the FTIR-based method and was considered throughout the quantitative model development to estimate the $CaCO_3$ content in cement.

2.4.6. Fourier transform infrared spectroscopy (FTIR)

Fourier transform infrared (FTIR) spectra were obtained using a PerkinElmer Spectrum 100 instrument with a Universal Attenuated Total Reflectance (ATR) accessory. The ATR consists of diamond/ZnSe crystal (1 reflection), top plate and pressure arm with force indicator. FTIR spectra were recorded in the range of 4000 to 650 cm^{-1}, resolution of 4 cm^{-1}, 16 scans and triplicate analysis. Clean ATR diamond/ZnSe crystal was used to record the background spectra.

2.4.7. Preparation of cement powder mixtures

The samples for calibration (C1-C11) and validation (V1-V10) of the FTIR-based method for $CaCO_3$ quantification were prepared from a physical mixture between non-carbonated (C1 – 45.80 mg $CaCO_3$/g cement) and carbonated (C11 – 468.20 mg $CaCO_3$/g cement) samples. All mixtures are detailed in Table 2. The application domain of the multivariate model covers the range of 45.80 to 468.20 mg $CaCO_3$/g cement. For model calibration, triplicates of non-carbonated (C1) and carbonated (C11) samples were obtained from the homogenized sample quartering. In addition, triplicate was prepared for each calibration mixture (C2-C10), while a duplicate was prepared for each point in the validation set (V1-V10). Thus, 33 samples and 99 FTIR spectra comprise the calibration set, while 20 samples and 60 FTIR spectra compose the validation set.

2.5. Data analysis

The data analysis was performed by means of partial least squares (PLS) regression in the software Solo + MIA (Eigenvector Research). Thus, PLS regression was applied to develop the model to quantify $CaCO_3$ in cement. The method is briefly detailed below.

2.5.1. Partial least squares (PLS) regression

Partial least squares (PLS) regression is the multivariate method applied to develop quantitative models. Thus, PLS aims to evaluate the

Table 2
Cement powder calibration and validation sets applied in the multivariate model.

Calibration set		Validation set	
Sample	mg $CaCO_3$/g cement	Sample	mg $CaCO_3$/g cement
C1_1	45.80	V1_1	67.17
C1_2	45.80	V1_2	69.92
C1_3	45.80	V2_1	110.96
C2_1	88.73	V2_2	110.69
C2_2	88.60	V3_1	152.11
C2_3	88.39	V3_2	152.38
C3_1	132.68	V4_1	193.25
C3_2	131.98	V4_2	193.81
C3_3	130.68	V5_1	235.74
C4_1	173.74	V5_2	236.46
C4_2	173.56	V6_1	276.66
C4_3	171.82	V6_2	278.50
C5_1	214.56	V7_1	319.58
C5_2	215.60	V7_2	319.65
C5_3	216.08	V8_1	360.40
C6_1	256.50	V8_2	360.45
C6_2	257.48	V9_1	403.45
C6_3	258.13	V9_2	404.29
C7_1	298.13	V10_1	445.33
C7_2	298.43	V10_2	445.92
C7_3	298.65		
C8_1	339.80		
C8_2	340.57		
C8_3	341.35		
C9_1	380.95		
C9_2	381.09		
C9_3	382.80		
C10_1	422.69		
C10_2	425.26		
C10_3	425.62		
C11_1	468.20		
C11_2	468.20		
C11_3	468.20		

relationship between predictive variables (X) and response properties (Y) through latent variables (factors) and load weights, optimizing the covariance relationship (X/Y) and establishing a regression. In the present work, the pre-processing of the FTIR spectra was carried out through the mean centering (MC), baseline correction (BC), standard normal variate (SNV) normalization and first derivative (1st Der).

3. Results and discussion

The results and discussions of the present work were divided between: (*i*) the carbonation reaction of the cylindrical cement specimens by supercritical CO_2, (*ii*) the carbonation reaction of the cement powder (C1) by supercritical CO_2 and (*iii*) the development of the multivariate analysis models based on FTIR spectra of non-carbonated (C1) and carbonated (C11) cement mixtures. For brevity purposes, the results of the carbonation study of cylindrical cement specimens are presented in Supplementary Material (Pages S12-S17).

3.1. Carbonation of cement powder

After evaluating the effect of supercritical CO_2 on cylindrical cement specimens (Supplementary Material), the carbonation process was accelerated from the reaction of CO_2 with powdered cement. The high surface area of the powdered cement reduces the time required for the carbonation process to achieve high conversions of the CH and C-S-H phases and produce a large amount of $CaCO_3$ and siliceous products [31]. Thus, the non-carbonated cement powder (C1) was obtained from the grinding of class G cement specimens, while the carbonated cement powder (C11) was obtained from the reaction of sample C1 with supercritical CO_2. Then, both samples (C1 and C11) were extensively characterized by XRD diffraction, SEM microscopy and FTIR spectroscopy.

3.1.1. Cement powder XRD analysis

Initially, non-carbonated (C1) and carbonated (C11) cement powders were analyzed by XRD diffraction. XRD was applied to identify the cement crystalline mineral components, although there is considerable amorphous fraction in the material [9,43,65]. Fig. 2 shows the XRD diffraction pattern, and the Supplementary Material (Table S3) presents the estimated mineral content of the crystalline fraction.

From the XRD pattern (Fig. 2A and Table S3) of the non-carbonated cement powder (C1), it was possible to observe that cement presents a greater diversity of crystalline components, characterized by: (*i*) unhydrated cement phases, composed of C_3S (Ca_3SiO_5 - Alite) and calcium aluminum iron oxide ($Ca_2Fe_{1.5}Al_{0.5}O_5$), (*ii*) cement hydration products, from the presence of portlandite (CH) and ettringite [$Ca_6Al_2(SO_4)_3(OH)_{12}{\cdot}26H_2O$] and (*iii*) a small fraction of calcite ($CaCO_3$ polymorph), resulting from the process of natural carbonation by atmospheric CO_2 throughout the sample preparation. No other $CaCO_3$ polymorph (amorphous, vaterite or aragonite) was identified. The observed profile is commonly described in the literature since a complete cure is unlikely and CH and ettringite are expected products of API class G cement hydration [3,10,19,66]. In addition, a small content of $CaCO_3$ is expected since it is unlikely to prevent the occurrence of natural carbonation [6,14,30]. Natural carbonation is explained by the reactivity of $Ca(OH)_2$ with atmospheric CO_2 and the difficulty of carrying out all sample preparation procedures (cement curing, grinding, sieving and storage) in inert environments. Furthermore, the calcium carbonate content for C1 (non-carbonated cement powder) was estimated as 45.80 mg $CaCO_3$/g cement, corresponding to 2.01 wt.% of CO_2 and 3.80% of carbonation degree.

On the other hand, from the XRD pattern (Fig. 2B and Table S3) of the carbonated cement powder (C11), it was confirmed that the sample undergoes a high degree of chemical transformation. It was observed that the crystalline fraction of C11 (carbonated cement powder) is basically composed of calcite ($CaCO_3$ polymorph). In addition, trace fractions of C_3S (Ca_3SiO_5 - Alite), calcium aluminum iron oxide ($Ca_2Fe_{1.5}Al_{0.5}O_5$) and quartz (SiO_2) are still identified, although they are not very representative in the composition of carbonated cement (C11). The carbonation process completely consumed portlandite (CH), being not identified in the C11 sample. The observed profile is commonly described in the literature since most carbonation products have amorphous characteristics [39,66–68]. In addition, from the XRD results, the $CaCO_3$ content of the C11 sample (carbonated cement) is significantly greater than what would be obtained from the single conversion of portlandite (CH). Thus, it was concluded that there is a high conversion of calcium silicate hydrate (C-S-H) to calcium carbonate and that both phases (CH and C-S-H) carbonation resulted in the formation of calcite polymorph. The preferential precipitation of the $CaCO_3$ polymorphs (calcite, aragonite and vaterite) is influenced by the reaction time, the carbonation degree and the other chemicals presence [11,41]. However, calcite is the most stable polymorph of calcium carbonate [69]. In this context, it is expected that in advanced stages of cement carbonation calcite will be the predominant $CaCO_3$ polymorph, being produced by precipitation and transformation processes of other calcium carbonate compounds (amorphous, vaterite and aragonite) [30,42–43]. Furthermore, the calcium carbonate content for C11 (carbonated cement powder) was estimated as 468.20 mg $CaCO_3$/g cement, corresponding to 20.59 wt.% of CO_2 and 38.82% of carbonation degree (approximately 10 times greater than in the C1 sample). Thus, these values found for C1 and C11 samples should be considered to develop a quantitative model based on FTIR.

3.1.2. Cement powder SEM microscopy

After characterizing the mineral composition of the non-carbonated (C1) and carbonated (C11) cement powders, SEM was applied to perform the materials morphological analysis (see Fig. 3).

From the non-carbonated cement (C1) SEM images (Fig. 3A and 3B), only pulverized calcium silicate hydrate was identified. Although C-S-H

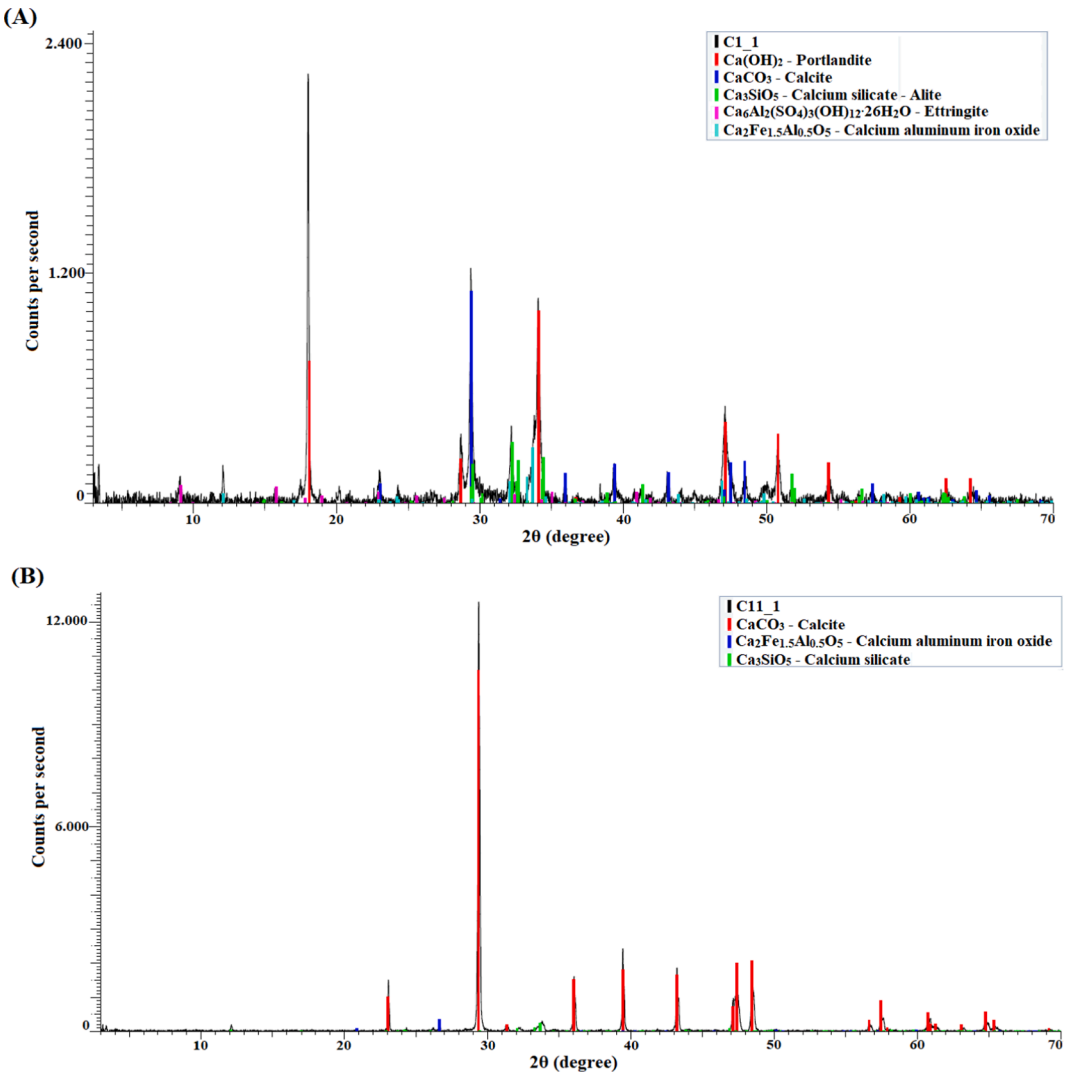

Fig. 2. XRD diffraction pattern of non-carbonated (C1) and carbonated (C11) cement powders.

gel is the major responsible for the development of mechanical strength of the cement [46,70], due to its low crystallinity and absence of preferential plans for cleavage of the mineral [19,67], the ball milling process results in a powder fraction containing particles with irregular shapes and different sizes. In addition, no additional components (CH, C_3S and $CaCO_3$), as identified by XRD diffraction (Fig. 2 and Table S3), could be observed in the analyzed fraction. On the other hand, from the carbonated cement (C11) SEM images (Fig. 3C and 3D), it was possible to observe some decalcified C-S-H and amorphous silica grains that were covered by poorly-crystalline calcite ($CaCO_3$) [42,71]. Calcite, identified in the XRD pattern, is characterized by its crystalline morphological structure. However, it requires long reaction times and slow precipitation processes to achieve its regular crystalline structure [71]. In addition, as observed in carbonated cylindrical cement specimens (Supplementary Material), $CaCO_3$ precipitates around the silica-rich phase (decalcified C-S-H and amorphous silica) were evidenced, resulting in a delay in the leaching process due to the passivation conferred by $CaCO_3$ covering the unreacted C-S-H [30,41,68].

3.1.3. *Cement powder FTIR analysis*

Fourier Transform Infrared Spectroscopy (FTIR) is a fast, low-cost, accurate and widely available method in universities and service and research laboratories [8,38–39]. FTIR scans the sample with a specified range of the electromagnetic radiation spectrum at the mid-infrared wavelength [72]. The profile of the IR spectra, recorded by the equipment as percentage of transmittance (% T) or percentage of absorbance (% A) versus wavenumber (cm^{-1}), is used to characterize molecular functional groups of the materials [19,62]. Since the molecular vibrational energy is quantized, each peak in the IR spectrum denotes the presence of a specific molecular functional group, while the relative intensity of the absorbed radiation (*i.e.*, height of the infrared peak) can be directly related to its concentration [19,73].

Several applications of FTIR were proposed in the literature to qualify or quantify minerals components in rocks, sediments, soil, and cement or to study transformation processes (*i.e.*, hydration, degradation, carbonation, etc.) in cementitious materials [39–40,46,74]. In this context, the use of Attenuated Total Reflectance (ATR) accessory is especially interesting for FTIR analysis, eliminating and simplifying sample preparations steps, favoring the analysis reproducibility, and increasing the method sensitivity [32,39–40,49,74]. Thus, the ATR-FTIR analysis presents all requirements for application in studies of cementitious materials, supporting the development of qualitative and quantitative methods, enabling quick, reliable, and low-cost evaluations of transformation processes, such as carbonation.

The present work proposes to use ATR-FTIR to: (*i*) study the carbonation process of cement by supercritical CO_2, (*ii*) evaluate changes in the IR spectral profile in mixtures of non-carbonated cement (C1) and carbonated (C11) cement powders and (*iii*) develop a

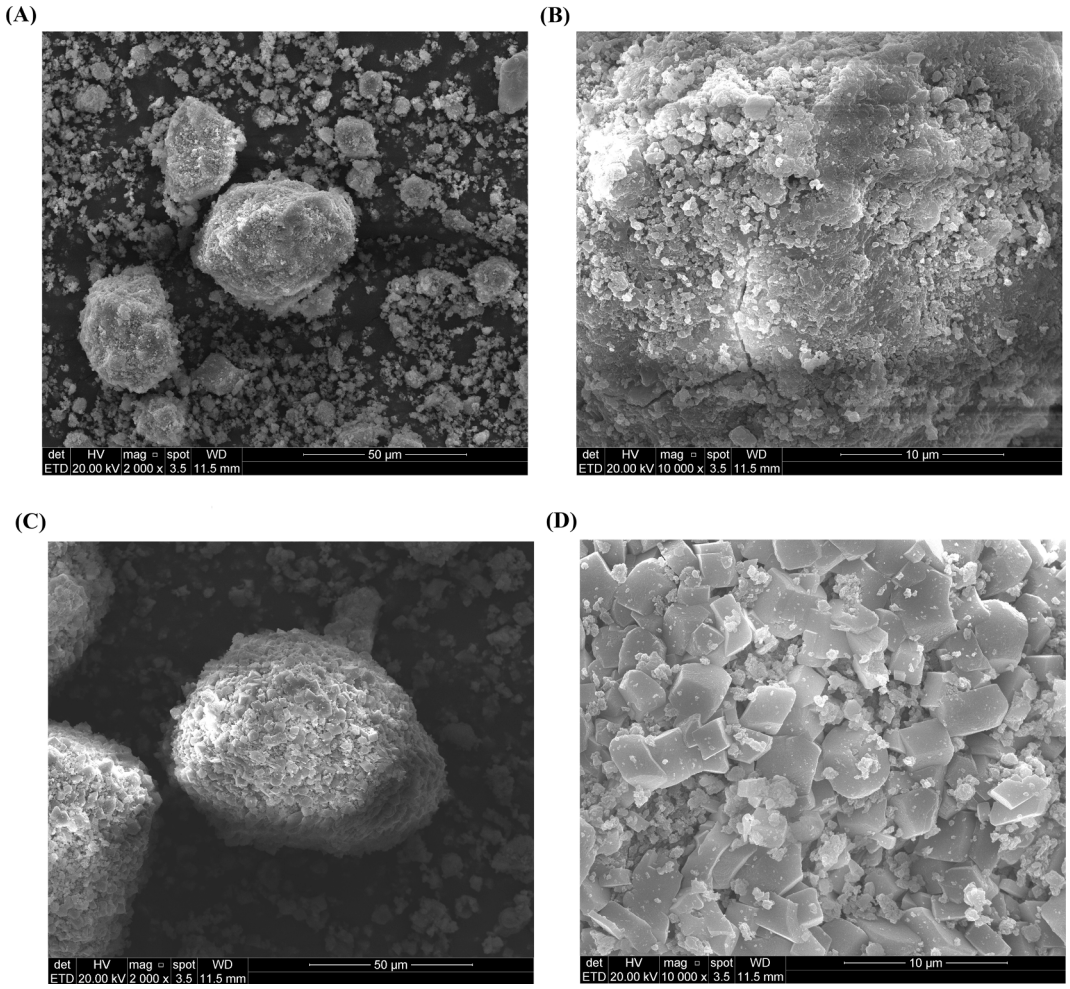

Fig. 3. SEM image of the non-carbonated (C1) and carbonated (C11) cement powders. Magnification of the cement powders: (A) C1 at 2000x, (B) C1 at 10000x, (C) C11 at 2000x and (D) C11 at 10000x.

quantitative method for $CaCO_3$ analysis in cement. Thus, API class G cement was used as reference material. The reference material was cured as recommended by the American Petroleum Institute (API) specification 10A [57], and then subjected to the carbonation process with supercritical CO_2 (at 65 °C, 15 MPa and 7 days). Fig. 4 shows the FTIR spectra of non-carbonated (C1) and carbonated (C11) cement powders.

From the FTIR spectral profile of the non-carbonated sample (C1), it

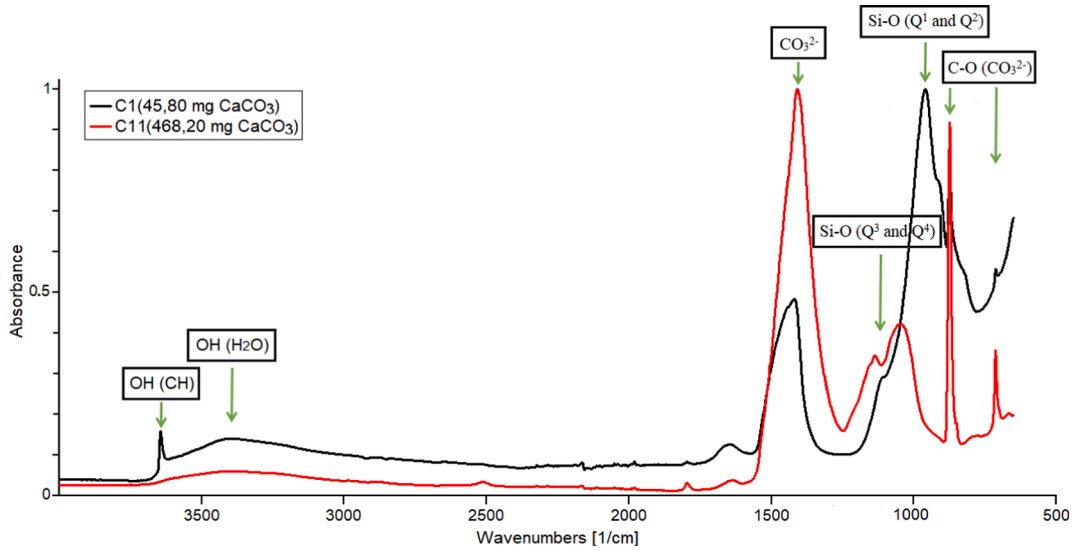

Fig. 4. FTIR spectra of non-carbonated (C1) and carbonated (C11) cement powders.

was possible to describe the following characteristics: (*i*) the presence of the peak related to the OH stretching of portlandite (CH) at 3640 cm^{-1}, (*ii*) a broadband at the 3600–3100 cm^{-1} range, attributed to the OH stretching of the water associated with the cement matrix, (*iii*) a small peak at 1640 cm^{-1}, attributed to bending vibration of water in sulfates, (*iv*) the carbonate (CO_3^{2-}) peaks at 1410 cm^{-1} (asymmetric C-O stretching), 873 cm^{-1} (out-of-plane vibration) and 713 cm^{-1} (in-plane vibration), associated with calcite ($CaCO_3$ polymorph) and (*v*) a broadband (800–1200 cm^{-1}), centered at 960 cm^{-1}, assigned to the Si-O asymmetric stretching (υ_3) of Q^1 and Q^2 species of calcium silicate hydrate (C-S-H) [34,39,65,70,75–76]. Thus, all the characteristics expected for API class G cement after curing was identified in the FTIR spectrum of the non-carbonated sample (C1). In addition, the result reinforces the occurrence of the natural carbonation process and confirms that the ATR-FTIR is sensitive to identify low contents of $CaCO_3$ (C1 – 45.80 mg $CaCO_3$/g cement) in cementitious material.

In contrast, from the FTIR spectral profile of the carbonated cement (C11), it was possible to highlight the following characteristics: (*i*) a broadband at the 3600–3100 cm^{-1} range, attributed to the OH stretching of the water associated with the cement matrix, (*ii*) a small peak at 1640 cm^{-1}, attributed to bending vibration of water in sulfates, (*iii*) the carbonate (CO_3^{2-}) peaks at 1410 cm^{-1} (asymmetric C-O stretching), 873 cm^{-1} (out-of-plane vibration) and 713 cm^{-1} (in-plane vibration), associated with calcite ($CaCO_3$ polymorph), in addition to weak peaks observed around 1790 cm^{-1} and 2518 cm^{-1} and (*iv*) a broadband (1250–900 cm^{-1}), centered at 1140 cm^{-1} and 1050 cm^{-1}, assigned to the Si-O asymmetric stretching (υ_3) of the decalcified C-S-H (Q^3 at 1050 cm^{-1}) and polymerized silica (Q^4 at 1140 cm^{-1}) phases [39,43,46,65,70,75,77]. Thus, the FTIR spectrum of the carbonated sample (C11) confirms the XRD data (Fig. 2 and Table S3) and indicates the total consumption of CH by the disappearance of the OH elongation at 3640 cm^{-1}, with the production of calcite, from the increase in the carbonate (CO_3^{2-}) peaks at 1410 cm^{-1} (asymmetric C-O stretching), 873 cm^{-1} (out-of-plane vibration) and 713 cm^{-1} (in-plane vibration). In addition, the position and intensity shift of the Si-O asymmetric stretching (υ_3) was observed from the non-carbonated sample (C1), centered at 960 cm^{-1}, to the carbonated sample (C11), centered at 1140 cm^{-1} and 1050 cm^{-1} [75]. These changes indicate the consumption of Q^1 and Q^2 species of calcium silicate hydrate (C-S-H) of non-carbonated cement powder by the carbonation process, resulting in a decalcification-polymerization process of C-S-H (Q^1 and Q^2) and leading to the production of decalcified C-S-H (Q^3) and polymerized silica (Q^4) phases [9,11,43]. Q^3 species are characterized by C-S-H with a lower Ca/Si ratio and cross-linked silicate tetrahedra, while Q^4 species are defined as amorphous silica with a highly condensed network of silicate tetrahedrons [9,34,43,65].

After the initial assessment of non-carbonated (C1) and carbonated (C11) cement powders, several intermediate mixtures were prepared from the mixture of C1 and C11, as detailed in Table 2. From the FTIR results (Fig. 4), it was observed that the spectral range (1700 to 650 cm^{-1}) comprises the main transformations of the cement matrix induced by the carbonation process. Thus, the ATR-FTIR sequential analyzes, representative of the calibration samples (C1-C11), are shown in Fig. 5.

In Fig. 5, the evolution of the FTIR spectrum profile is observed as the carbonated (C11) fraction of the mixture increases. Thus, the following most relevant characteristics are observed: (*i*) the increase in the carbonate (CO_3^{2-}) peaks at 1410 cm^{-1} (asymmetric C-O stretching), 873 cm^{-1} (out-of-plane vibration) and 713 cm^{-1} (in-plane vibration) of the calcite, (*ii*) decalcification-polymerization of the C-S-H chain, leading to a shift in the broadband attributed to Si-O asymmetric stretching from 800 to 1200 cm^{-1} (Q^1 and Q^2 species) to a higher wavenumber range 1250–900 cm^{-1} (Q^3 and Q^4 species), (*iii*) reduction of the relative intensities of the Si-O asymmetric stretching due to the polymerization process of the silicate phases [34,46,75], and (*iv*) reduction in the detection interference of the carbonate peaks (873 cm^{-1} and 713 cm^{-1}) due to the overlapping effect caused by C-S-H (Q^1 and Q^2 species). Thus,

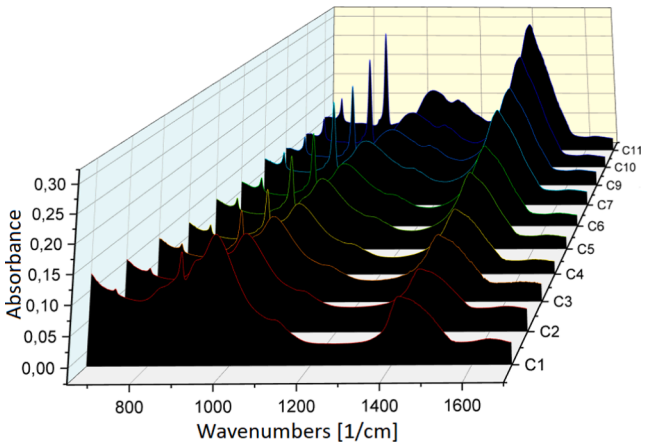

Fig. 5. Sequential modification of FTIR spectra of cement powder mixtures.

the increase in the intensity of specific $CaCO_3$ bands and the reduction of interference from other cement components indicate that it was possible to develop methods to quantify $CaCO_3$ in cement by ATR-FTIR.

From the analysis of non-carbonated cement (C1), carbonated cement (C11), and its mixtures (C2-C10), it was possible to: (*i*) evaluate the changes resulting from the carbonation process with supercritical CO_2, (*ii*) identify the spectral profile of non-carbonated (C1) and carbonated (C11) cement, (*iii*) confirm the potential of ATR-FTIR to analyze cementitious materials, (*iv*) perform a clear identification of $CaCO_3$ and (*v*) relate the intensity of the absorbed radiation to the cement components concentration. In addition, complementing the previous information provided by MicroCT (Figure S4), SEM-EDS (Figure S5 and Fig. 3) and XRD (Fig. 2 and Table S3), ATR-FTIR was able to identify changes in the siliceous fraction of cement, usually studied by the expensive ^{29}Si NMR.

3.2. Multivariate analysis

Based on the IR results, ATR-FTIR shows to be an adequate method to develop fast, reliable, and low-cost quantitative models for the characterization of cementitious materials. Continuous variables, such as FTIR spectra, are incredibly informative and compatible with multivariate analysis tools. Thus, applying the MVA methods, it was possible to identify the IR spectrum regions that best fit to the intended response. In this context, to obtain reliable quantitative models, special attention is required to pre-process the FTIR spectra and the calibration and validation procedures. Thus, the development of a predictive model to quantify $CaCO_3$ in cement was evaluated from the application of partial least squares (PLS) regression. To develop the MVA models, the pre-processing of the FTIR spectra were performed through the mean centering (MC), baseline correction (BC), standard normal variate (SNV) normalization and first derivative (1st Der). Therefore, three PLS models were developed evaluating different combinations of pre-processing of the infrared spectra, which are: (Model 1) mean centering (MC) and baseline correction (BC), (Model 2) MC, BC, and standard normal variate (SNV) normalization and (Model 3) MC, BC, SNV and first derivative (1st Der). Thus, the PLS models were calibrated (C1 to C11) and evaluated with an independent validation set (V1-V10). From the validation set, consisting of samples not included in the calibration, it was possible to: (*i*) avoid an optimum evaluation of the results, (*ii*) confirm the predictive capacity of the model and (*iii*) guarantee the transferability of experimental procedures to characterize carbonated cement by ATR-FTIR. Thus, the PLS models (calibration and validation) to quantify $CaCO_3$ in cement are shown in Table 3. At the same time, the reference and predicted values are presented in the Supplementary Material (Table S4).

From Table 3, it was observed that all developed PLS models used 6

Table 3
Parameters obtained for PLS regression models.

Parameters	PLS		
	Model 1	Model 2	Model 3
Pre-processing	MC; BC	MC; BC; SNV	MC; BC; SNV; 1st Der
Factors	6	6	6
EV% (X/y)	99.96	99.82	99.59
R^2 Calibration	0.9981	0.9996	0.9997
R^2 Prediction	0.9975	0.9993	0.9995
RMSEC	5.85	2.81	2.41
RMSEP	11.85	4.13	3.61
Calibration Bias	0.00	0.00	0.00
Prediction Bias	8.79	2.50	2.37

EV - Explained variance; RMSEC - Root Mean Square Error of Calibration; RMSEP - Root Mean Square Error of Prediction; MC - mean centered; BC - baseline correction; SVN - standard normal variate; 1st Der - first derivative transformation.

factors (LV) for the calibration, resulting in a total of 99.96% (Model 1), 99.82% (Model 2), and 99.59% (Model 3) of explained variance. From the calibration set, good correlation coefficients (R^2) were obtained for Model 1 (R^2 = 0.9981), Model 2 (R^2 = 0.9996) and Model 3 (R^2 = 0.9997). In addition, regression modeling resulted in low root mean square error of calibration (RMSEC) for Model 1 (RMSEC = 5.85 mg $CaCO_3$/g cement), Model 2 (RMSEC = 2.81 mg $CaCO_3$/g cement) and Model 3 (RMSEC = 2.41 mg $CaCO_3$/g cement) and bias close to 0. However, the final evaluation of multivariate regression models must be performed based on an independent validation set. Thus, from Table 3, it was observed that the correlation coefficients (R^2) were obtained from the application of Model 1 (R^2 = 0.9975), Model 2 (R^2 = 0.9993) and Model 3 (R^2 = 0.9995) also showed good regression adjustment. From the validation set, low root mean square errors of prediction (RMSEP) and good bias values were obtained for Model 1 (RMSEP = 11.85 mg $CaCO_3$/g cement; bias = 8.79 mg $CaCO_3$/g cement), Model 2 (RMSEP = 4.13 mg $CaCO_3$/g cement; bias = 2.50 mg $CaCO_3$/g cement) and Model 3 (RMSEP = 3.61 mg $CaCO_3$/g cement; bias = 2.37 mg $CaCO_3$/g cement). Thus, it was concluded that it is possible to calibrate PLS regressions with minimum requirements to quantify $CaCO_3$ in cement using ATR-FTIR, which are: (*i*) correlation coefficients (R^2) close to 1, (*ii*) low estimation errors (RMSEC and RMSEP) and (*iii*) low bias values (calibration bias and prediction bias). Thus, after the initial assessment, Model 3 was selected for a more comprehensive interpretation, as it presents the best PLS regression outputs. The results are shown in Fig. 6.

From Fig. 6A, it was possible to observe the good correlation coefficient (R^2 = 0.9995) from the "predicted vs. reference" plot of PLS (Model 3). The "residual plot" (Fig. 6B) shows the difference between the predicted and the reference values. No systematic error can be observed, with the values being distributed randomly around 0. Furthermore, from the PLS loading (Fig. 6C and 6D), it was possible to identify the most important regions of the FTIR spectrum to quantify

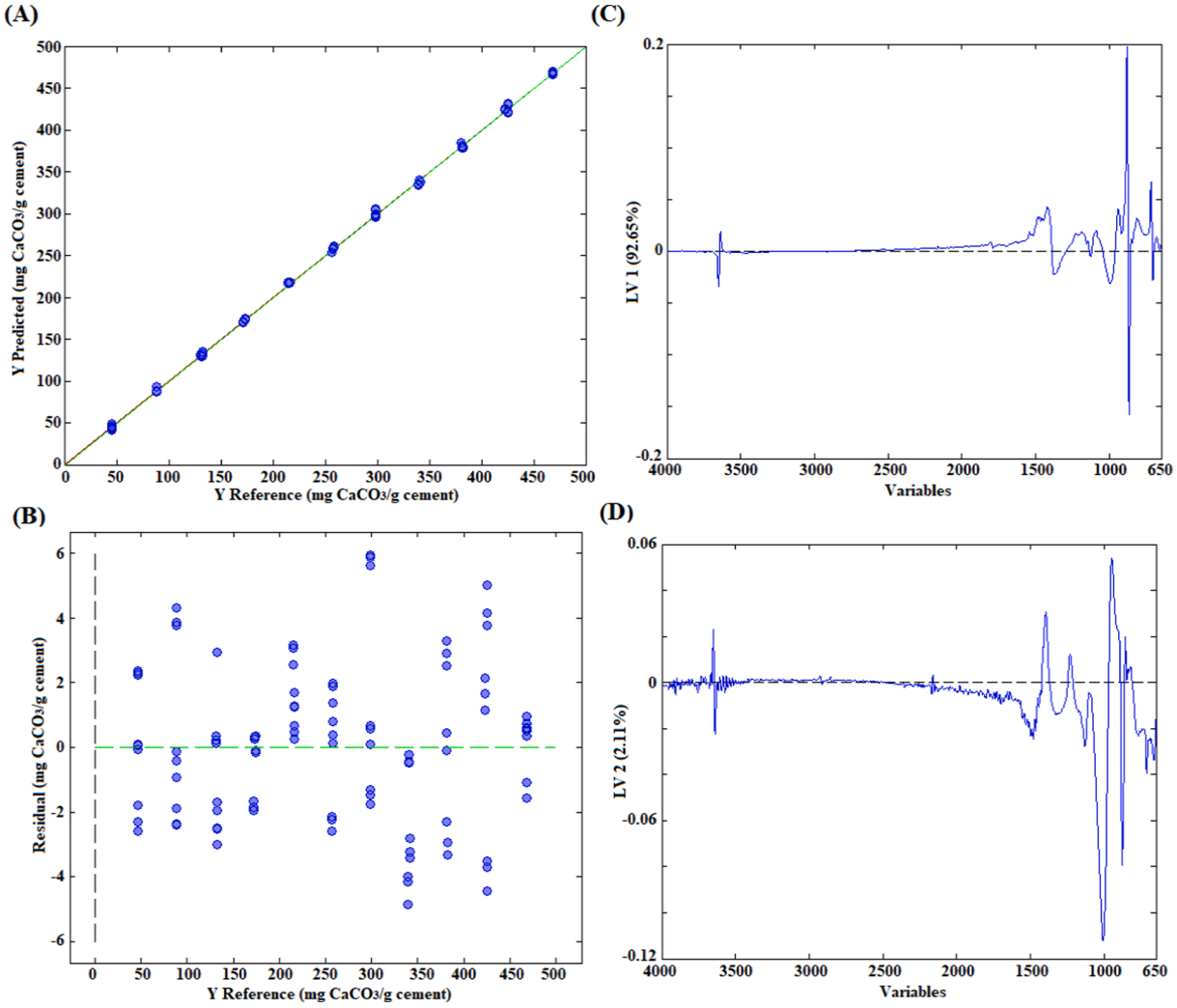

Fig. 6. PLS regression analysis from FTIR spectra of cement powders to quantify $CaCO_3$: (A) predicted vs. reference plot, (B) residual plot, (C) PLS loading (LV 1) and (D) PLS loading (LV 2).

$CaCO_3$ in cement. The spectral regions and characteristics most relevant to the PLS regression are: (*i*) the consumption of portlandite (CH), with the reduction in OH stretching at 3640 cm^{-1}, (*ii*) the increase in the carbonate (CO_3^{2-}) peaks at 1410 cm^{-1} (asymmetric C-O stretching), 873 cm^{-1} (out-of-plane vibration) and 713 cm^{-1} (in-plane vibration) and (*iii*) the displacement of the Si-O asymmetric stretching from 800 to 1200 cm^{-1} (Q^1 and Q^2 species) to 1250–900 cm^{-1} (Q^3 and Q^4 species) due to the decalcification-polymerization of the calcium silicate hydrate (C-S-H) chain throughout the carbonation process.

It was concluded that it is possible to develop reliable PLS models to quantify $CaCO_3$ in cement by ATR-FTIR. The experimental advantages of ATR-FTIR cement powder analysis are: (*i*) eliminate sample preparation steps, (*ii*) reduce the analysis time, (*iii*) eliminate the KBR use, (*iv*) reduce the analysis costs, (*v*) improve the reproducibility of the method and (*vi*) mitigate the occurrence of operator errors. In addition, the analysis time of the ATR-FTIR (a few minutes) is significantly shorter than the TGA (a few hours) and the average percentage of Model 3 prediction error (±2.75%) is lower than that obtained by thermogravimetric analysis (±5%) [41,43]. Furthermore, from the interpretation of the PLS, it was observed that it is necessary to consider the global effect of the carbonation process in the cement matrix to obtain reliable models, since the chemical transformations significantly change the profile of the infrared spectra. The most important processes are: (*i*) the consumption of portlandite (CH), (*ii*) the decalcification-polymerization process of calcium silicate hydrate (C-S-H) and (*iii*) the increase in the $CaCO_3$ content.

4. Conclusions

Partial least squares (PLS) regression models were developed to quantify $CaCO_3$ in cement and to study the CO_2 effect on the material matrix. PLS models were calibrated and validated, and the regression results presented good correlation coefficient ($R^2 = 0.9995$) and low estimation error (RMSEP = 3.61 mg $CaCO_3$/g cement). From the results, it was observed that the portlandite (CH) consumption, the increase in $CaCO_3$ content and the C-S-H decalcification-polymerization are the most relevant chemical transformations of cement throughout the carbonation process. Thus, it was concluded that: *i*) it is possible to obtain fast, low-cost, and reliable models to quantify $CaCO_3$ by FTIR and *ii*) the method is applicable to study carbonated cement-based materials.

The results of the present work show that it is necessary to consider the physical and chemical transformations induced by the carbonation process in the cement matrix to develop reliable quantitative models to estimate the $CaCO_3$ content in the material. To expand the scope of application of the FTIR-based method for the analysis of carbonated cementitious materials, future studies should: (*i*) reproduce the experimental procedure with other types of cement, (*ii*) evaluate the influence of the carbonation type (natural, accelerated, or supercritical) or the exposure stage (carbonation cure or cement degradation) on the model and (*iii*) study the effect of other $CaCO_3$ polymorphs on the performance of the method.

CRediT authorship contribution statement

Victor Hugo Jacks Mendes dos Santos: Conceptualization, Methodology, Software, Validation, Formal analysis, Investigation, Data curation, Writing – original draft, Writing – review & editing, Visualization. **Darlan Pontin:** Methodology, Formal analysis, Investigation, Writing – review & editing. **Gabriela Gonçalves Dias Ponzi:** Methodology, Formal analysis, Investigation, Writing – review & editing. **Amanda Sofia de Guimarães e Stepanha:** Methodology, Formal analysis, Investigation, Writing – review & editing. **Renan Bordulis Martel:** Methodology, Formal analysis, Investigation, Writing – review & editing. **Marta Kerber Schütz:** Conceptualization, Validation, Formal analysis, Investigation, Writing – review & editing, Visualization. **Sandra Mara Oliveira Einloft:** Conceptualization, Validation, Formal analysis, Investigation, Writing – review & editing, Visualization. **Felipe Dalla Vecchia:** Conceptualization, Methodology, Validation, Formal analysis, Investigation, Resources, Writing – review & editing, Visualization, Supervision, Project administration, Funding acquisition.

Declaration of Competing Interest

The authors declare that they have no known competing financial interests or personal relationships that could have appeared to influence the work reported in this paper.

Acknowledgments

The authors would like to thank the Institute of Petroleum and Natural Resource (IPR) of the Pontifical Catholic University of Rio Grande do Sul for the infrastructure, Dra. Rosalia Barili da Cunha for help with the XRD diffraction analyzes interpretation and Lafarge Holcim for the donation of the cement. This study was financed in part by the Coordenação de Aperfeiçoamento de Pessoal de Nível Superior – Brasil (CAPES) – Finance Code 001. In addition, this work was supported by Petrobras (grant numbers: 2017/00742-8 and 2018/00235-1) and by ANP (Brazil's National Oil, Natural Gas and Biofuels Agency), through the R&D levy regulation.

Appendix A. Supplementary material

Supplementary data to this article can be found online at https://doi.org/10.1016/j.conbuildmat.2021.125413.

References

[1] T. Wilberforce, A.G. Olabi, E.T. Sayed, K. Elsaid, M.A. Abdelkareem, Progress in carbon capture technologies, Sci. Total Environ. 761 (2021) 143203, https://doi.org/10.1016/j.scitotenv.2020.143203.
[2] M. Bai, J. Sun, K. Song, K.M. Reinicke, C. Teodoriu, Evaluation of mechanical well integrity during CO_2 underground storage, Environ, Earth Sci. 73 (11) (2015) 6815–6825, https://doi.org/10.1007/s12665-015-4157-5.
[3] L. Liu, Y. Ji, F. Gao, L.i. Zhang, Z. Zhang, XiangYu Liu, Study on high-efficiency CO_2 absorption by fresh cement paste, Constr. Build. Mater. 270 (2021) 121364, https://doi.org/10.1016/j.conbuildmat.2020.121364.
[4] R.M. Andrew, Global CO_2 emissions from cement production, Earth Syst. Sci. Data. 10 (2018) 195–217, https://doi.org/10.5194/essd-10-195-2018.
[5] B. Metz, O. Davidson, H. De Coninck, M. Loos, L. Meyer. IPCC special report on carbon dioxide capture and storage, Working Group III of the Intergovernmental Panel on Climate Change, Cambridge University Press, Cambridge, United Kingdom and New York, NY, USA, 2005, pp. 442–pp.
[6] E. Benhelal, E. Shamsaei, M.I. Rashid, Challenges against CO_2 abatement strategies in cement industry: A review, J. Environ. Sci. 104 (2021) 84–101, https://doi.org/10.1016/j.jes.2020.11.020.
[7] L. Mazurana, P.R.S. Bittencourt, F.R. Scremin, A. Neves Junior, E. Possan, Determination of CO_2 capture in rendering mortars produced with recycled construction and demolition waste by thermogravimetry, J. Therm. Anal. Calorim. (2021), https://doi.org/10.1007/s10973-020-10436-0.
[8] T. Shi, Y. Gao, D.J. Corr, S.P. Shah, FTIR study on early-age hydration of carbon nanotubes-modified cement-based materials, Adv. Cem. Res. 31 (8) (2019) 353–361, https://doi.org/10.1680/jadcr.16.00167.
[9] W. Ashraf, Carbonation of cement-based materials: Challenges and opportunities, Constr. Build. Mater. 120 (2016) 558–570, https://doi.org/10.1016/j.conbuildmat.2016.05.080.
[10] B.L.d.S. Costa, J.C.d.O. Freitas, D.M.d.A. Melo, R.G.d.S. Araujo, Y.H.d. Oliveira, C. A. Simão, Evaluation of density influence on resistance to carbonation process in oil well cement slurries, Constr. Build. Mater. 197 (2019) 331–338, https://doi.org/10.1016/j.conbuildmat.2018.11.232.
[11] W. Liu, Y.-Q. Li, L.-P. Tang, Z.-J. Dong, XRD and ^{29}Si MAS NMR study on carbonated cement paste under accelerated carbonation using different concentration of CO_2, Mater. Today Commun. 19 (2019) 464–470, https://doi.org/10.1016/j.mtcomm.2019.05.007.
[12] F. Dalla Vecchia, V.H.J.M. dos Santos, M.K. Schütz, G.G.D. Ponzi, A.S.d.G. e. Stepanha, C.d.F. Malfatti, E.M.d. Costa, Wellbore integrity in a saline aquifer: Experimental steel-cement interface degradation under supercritical CO_2 conditions representative of Brazil's Parana basin, Int. J. Greenh. Gas Control. 98 (2020) 103077, https://doi.org/10.1016/j.ijggc.2020.103077.
[13] B. Liu, J. Qin, J. Shi, J. Jiang, X. Wu, Z. He, New perspectives on utilization of CO_2 sequestration technologies in cement-based materials, Constr. Build. Mater. 272 (2021), 121660, https://doi.org/10.1016/j.conbuildmat.2020.121660.

[14] S.O. Ekolu, A review on effects of curing, sheltering, and CO_2 concentration upon natural carbonation of concrete, Constr. Build. Mater. 127 (2016) 306–320, https://doi.org/10.1016/j.conbuildmat.2016.09.056.

[15] G.G.D. Ponzi, V.H.J.M.D. Santos, R.B. Martel, D. Pontin, A.S.d.G.e. Stepanha, M. K. Schütz, S.C. Menezes, S.M.O. Einloft, F.D. Vecchia, Basalt powder as a supplementary cementitious material in cement paste for CCS wells: chemical and mechanical resistance of cement formulations for CO_2 geological storage sites, Int. J. Greenh. Gas Control. 109 (2021) 103337, https://doi.org/10.1016/j.ijggc.2021.103337.

[16] S. Yadav, A. Mehra, A review on ex situ mineral carbonation, Environ. Sci. Pollut. Res. 28 (10) (2021) 12202–12231, https://doi.org/10.1007/s11356-020-12049-4.

[17] D. Zhang, Z. Ghouleh, Y. Shao, Review on carbonation curing of cement-based materials, J. CO_2 Util. 21 (2017) 119–131, https://doi.org/10.1016/j.jcou.2017.07.003.

[18] S. Salehi, J. Khattak, F.K. Saleh, S. Igbojekwe, Investigation of mix design and properties of geopolymers for application as wellbore cement, J. Pet. Sci. Eng. 178 (2019) 133–139, https://doi.org/10.1016/j.petrol.2019.03.031.

[19] O. Omosebi, H. Maheshwari, R. Ahmed, S. Shah, S. Osisanya, S. Hassani, G. DeBruijn, W. Cornell, D. Simon, Degradation of well cement in HPHT acidic environment: Effects of CO_2 concentration and pressure, Cem. Concr. Compos. 74 (2016) 54–70, https://doi.org/10.1016/j.cemconcomp.2016.09.006.

[20] J.M. Paris, J.G. Roessler, C.C. Ferraro, H.D. DeFord, T.G. Townsend, A review of waste products utilized as supplements to Portland cement in concrete, J. Clean. Prod. 121 (2016) 1–18, https://doi.org/10.1016/j.jclepro.2016.02.013.

[21] P. Šiler, I. Kolářová, T. Sehnal, R. Snop, T. Opravil, F. Šoukal, The Influence of Particle Size of Cement and Different Additives on the Properties of Portland Cement Pastes, Mater. Sci. Forum. 851 (2016) 104–109, https://doi.org/10.4028/www.scientific.net/MSF.851.104.

[22] M. Bagheri, S.M. Shariatipour, E. Ganjian, A review of oil well cement alteration in CO_2-rich environments, Constr. Build. Mater. 186 (2018) 946–968, https://doi.org/10.1016/j.conbuildmat.2018.07.250.

[23] A. Deshpande, R. Patil, Applications of Nanotechnology in Oilwell Cementing, in: SPE Middle East Oil Gas Show Conf., Society of Petroleum Engineers, 2017: pp. 6–9. doi:10.2118/183727-MS.

[24] M. Tiong, R. Gholami, M.E. Rahman, Cement degradation in CO_2 storage sites: a review on potential applications of nanomaterials, J. Pet. Explor. Prod. Technol. 9 (1) (2019) 329–340, https://doi.org/10.1007/s13202-018-0490-z.

[25] J. Hwang, R. Ahmed, S. Tale, S. Shah, Shear bond strength of oil well cement in carbonic acid environment, J. CO_2 Util. 27 (2018) 60–72, https://doi.org/10.1016/j.jcou.2018.07.001.

[26] T. Gu, X. Guo, Z. Li, X. Cheng, X. Fan, A. Korayem, W.H. Duan, Coupled effect of CO_2 attack and tensile stress on well cement under CO_2 storage conditions, Constr. Build. Mater. 130 (2017) 92–102, https://doi.org/10.1016/j.conbuildmat.2016.10.117.

[27] K. Abid, R. Gholami, H. Elochukwu, M. Mostofi, C.H. Bing, G. Muktadir, A methodology to improve nanosilica based cements used in CO_2 sequestration sites, Petroleum. 4 (2) (2018) 198–208, https://doi.org/10.1016/j.petlm.2017.10.005.

[28] S. Al Wakeel, J. Němeček, L. Li, Y. Xi, M. Hubler, The effect of introducing nanoparticles on the fracture toughness of well cement paste, Int. J. Greenh. Gas Control. 84 (2019) 147–153, https://doi.org/10.1016/j.ijggc.2019.03.009.

[29] E.-J. Moon, Y.C. Choi, Carbon dioxide fixation via accelerated carbonation of cement-based materials: Potential for construction materials applications, Constr. Build. Mater. 199 (2019) 676–687, https://doi.org/10.1016/j.conbuildmat.2018.12.078.

[30] B. Šavija, M. Luković, Carbonation of cement paste: Understanding, challenges, and opportunities, Constr. Build. Mater. 117 (2016) 285–301, https://doi.org/10.1016/j.conbuildmat.2016.04.138.

[31] S. Park, H. Moon, J.-H. Kim, M. Lee, C.-W. Chung, Reaction of hydrated cement paste with supercritical carbon dioxide, Constr. Build. Mater. 281 (2021) 122615, https://doi.org/10.1016/j.conbuildmat.2021.122615.

[32] M. Horgnies, J.J. Chen, C. Bouillon, Overview about the use of Fourier Transform Infrared spectroscopy to study cementitious materials, in, WIT Trans. Eng. Sci. (2013) 251–262, https://doi.org/10.2495/MC130221.

[33] R. Bjørge, K. Gawel, E.A. Chavez Panduro, M. Torsæter, Carbonation of silica cement at high-temperature well conditions, Int. J. Greenh. Gas Control. 82 (2019) 261–268, https://doi.org/10.1016/j.ijggc.2019.01.011.

[34] B. Wu, G. Ye, Study of carbonation rate of synthetic C-S-H by XRD, NMR and FTIR, Heron. 64 (2019) 21–38.

[35] K. Kupwade-Patil, S.D. Palkovic, A. Bumajdad, C. Soriano, O. Büyüköztürk, Use of silica fume and natural volcanic ash as a replacement to Portland cement: Micro and pore structural investigation using NMR, XRD, FTIR and X-ray microtomography, Constr. Build. Mater. 158 (2018) 574–590, https://doi.org/10.1016/j.conbuildmat.2017.09.165.

[36] A.R. Duggan, J. Goggins, E. Clifford, B.A. McCabe, The Use of Carbonation Depth Techniques on Stabilized Peat, Geotech. Test. J. 40 (6) (2017) 20160223, https://doi.org/10.1520/GTJ20160223.

[37] D. Gastaldi, F. Canonico, S. Irico, D. Pellerej, M.C. Paganini, Near-infrared spectroscopy investigation on the hydration degree of a cement paste, J. Mater. Sci. 45 (12) (2010) 3169–3174, https://doi.org/10.1007/s10853-010-4323-9.

[38] J.P. Rebouças, J.J.R. Rohwedder, C. Pasquini, Near infrared emission spectroscopy for rapid compositional analysis of Portland cements, Anal. Chim. Acta. 1024 (2018) 136–144, https://doi.org/10.1016/j.aca.2018.03.035.

[39] J. Higl, D. Hinder, C. Rathgeber, B. Ramming, M. Lindén, Detailed in situ ATR-FTIR spectroscopy study of the early stages of C-S-H formation during hydration of monoclinic C_3S, Cem. Concr. Res. 142 (2021) 106367, https://doi.org/10.1016/j.cemconres.2021.106367.

[40] D.G. Henry, J.S. Watson, C.M. John, Assessing and calibrating the ATR-FTIR approach as a carbonate rock characterization tool, Sediment. Geol. 347 (2017) 36–52, https://doi.org/10.1016/j.sedgeo.2016.07.003.

[41] K. Vance, G. Falzone, I. Pignatelli, M. Bauchy, M. Balonis, G. Sant, Direct Carbonation of Ca(OH)2 Using Liquid and Supercritical CO2: Implications for Carbon-Neutral Cementation, Ind. Eng. Chem. Res. 54 (2015) 8908–8918, https://doi.org/10.1021/acs.iecr.5b02356.

[42] R. Chang, S. Kim, S. Lee, S. Choi, M. Kim, Y. Park, Calcium Carbonate Precipitation for CO_2 Storage and Utilization: A Review of the Carbonate Crystallization and Polymorphism, Front. Energy Res. 5 (2017) 1–12, https://doi.org/10.3389/fenrg.2017.00017.

[43] M. Saillio, V. Baroghel-Bouny, S. Pradelle, M. Bertin, J. Vincent, J.-B. d'Espinose de Lacaillerie, Effect of supplementary cementitious materials on carbonation of cement pastes, Cem. Concr. Res. 142 (2021) 106358, https://doi.org/10.1016/j.cemconres.2021.106358.

[44] R. Schneider dos Santos, S.B.A. Rolim, F. Hepp Pulgati, Application of visible and near infrared spectroscopy in non-destructive evaluation of cement materials, Int. J. Remote Sens. 36 (3) (2015) 917–938, https://doi.org/10.1080/01431161.2014.1001083.

[45] P. Rosén, H. Vogel, L. Cunningham, N. Reuss, D.J. Conley, P. Persson, Fourier transform infrared spectroscopy, a new method for rapid determination of total organic and inorganic carbon and biogenic silica concentration in lake sediments, J. Paleolimnol. 43 (2) (2010) 247–259, https://doi.org/10.1007/s10933-009-9329-4.

[46] A. Jose, M.R. Nivitha, J.M. Krishnan, R.G. Robinson, Characterization of cement stabilized pond ash using FTIR spectroscopy, Constr. Build. Mater. 263 (2020) 120136, https://doi.org/10.1016/j.conbuildmat.2020.120136.

[47] Y. Otsuka, M. Takeuchi, M. Otsuka, B. Ben-Nissan, D. Grossin, H. Tanaka, Effect of carbon dioxide on self-setting apatite cement formation from tetracalcium phosphate and dicalcium phosphate dihydrate; ATR-IR and chemoinformatics analysis, Colloid Polym. Sci. 293 (10) (2015) 2781–2788, https://doi.org/10.1007/s00396-015-3616-6.

[48] S. Nasrazadani, T. Springfield, Application of Fourier transform infrared spectroscopy in cement Alkali quantification, Mater. Struct. 47 (10) (2014) 1607–1615, https://doi.org/10.1617/s11527-013-0140-3.

[49] S. Veerasingam, R. Venkatachalapathy, Estimation of carbonate concentration and characterization of marine sediments by Fourier Transform Infrared Spectroscopy, Infrared Phys. Technol. 66 (2014) 136–140, https://doi.org/10.1016/j.infrared.2014.06.005.

[50] A. Guatame-Garcia, M. Buxton, The Use of Infrared Spectroscopy to Determine the Quality of Carbonate-Rich Diatomite Ores, Minerals. 8 (2018) 120, https://doi.org/10.3390/min8030120.

[51] X. Liu, S.M. Colman, E.T. Brown, E.C. Minor, H. Li, Estimation of carbonate, total organic carbon, and biogenic silica content by FTIR and XRF techniques in lacustrine sediments, J. Paleolimnol. 50 (3) (2013) 387–398, https://doi.org/10.1007/s10933-013-9733-7.

[52] Y. Luzinova, G.T. Dobbs, L. Lapham, J.P. Chanton, B. Mizaikoff, Detection of cold seep derived authigenic carbonates with infrared spectroscopy, Mar. Chem. 125 (1-4) (2011) 8–18, https://doi.org/10.1016/j.marchem.2011.01.006.

[53] M. Mecozzi, E. Pietrantonio, M. Amici, G. Romanelli, Determination of carbonate in marine solid samples by FTIR-ATR spectroscopy, Analyst. 126 (2001) 144–146, https://doi.org/10.1039/b009031j.

[54] M. Tatzber, M. Stemmer, H. Spiegel, C. Katzlberger, G. Haberhauer, M. H. Gerzabek, An alternative method to measure carbonate in soils by FT-IR spectroscopy, Environ. Chem. Lett. 5 (1) (2007) 9–12, https://doi.org/10.1007/s10311-006-0079-5.

[55] M.A. Legodi, D. De Waal, J.H. Potgieter, Quantitative Determination of $CaCO_3$ in Cement Blends by FT-IR, Appl. Spectrosc. 55 (3) (2001) 361–365, https://doi.org/10.1366/0003702011951786.

[56] T.L. Hughes, C.M. Methven, T.G.J. Jones, S.E. Pelham, P. Fletcher, C. Hall, Determining cement composition by Fourier transform infrared spectroscopy, Adv. Cem. Based Mater. 2 (3) (1995) 91–104, https://doi.org/10.1016/1065-7355(94)00031-X.

[57] A.P.I. Specification, API 10A - Specification for Cements and Materials for Well Cementing, Am. Pet. Inst. 2009 (2010) 50, https://doi.org/10.1002/jcc.

[58] M.A. Celia, S. Bachu, J.M. Nordbotten, K.W. Bandilla, Status of CO_2 storage in deep saline aquifers with emphasis on modeling approaches and practical simulations, Water Resour. Res. 51 (9) (2015) 6846–6892, https://doi.org/10.1002/2015WR017609.

[59] C. Teodoriu, O. Bello, A review of cement testing apparatus and methods under CO_2 environment and their impact on well integrity prediction – Where do we stand? J. Pet. Sci. Eng. 187 (2020) 106736, https://doi.org/10.1016/j.petrol.2019.106736.

[60] A. Lavrov, Stiff cement, soft cement: Nonlinearity, arching effect, hysteresis, and irreversibility in CO_2-well integrity and near-well geomechanics, Int. J. Greenh. Gas Control. 70 (2018) 236–242, https://doi.org/10.1016/j.ijggc.2017.11.012.

[61] N. Koukouzas, Z. Kypritidou, C. Vasilatos, N. Tsoukalas, C.A. Rochelle, G. Purser, Geochemical modeling of carbonation of hydrated oil well cement exposed to CO_2-saturated brine solution, Appl. Geochemistry. 85 (2017) 35–48, https://doi.org/10.1016/j.apgeochem.2017.08.002.

[62] A. Ranjan, R. Kumar, D. Mohan, Comparative analysis of phenolphthalein indicator, XRDA and FTIR methods for measurement of carbonation depth of concrete, Int. J. Civ. Eng. Technol. 9 (2018) 315–320.

[63] T. Chen, M. Bai, X. Gao, Carbonation curing of cement mortars incorporating carbonated fly ash for performance improvement and CO_2 sequestration, J. CO_2 Util. 51 (2021) 101633, https://doi.org/10.1016/j.jcou.2021.101633.
[64] H.H. Steinour, Some effects of carbon dioxide on mortars and concrete-discussion, J. Am. Concr. Inst. 30 (1959) 905–907.
[65] J. Skocek, M. Zajac, M. Ben Haha, Carbon Capture and Utilization by mineralization of cement pastes derived from recycled concrete, Sci. Rep. 10 (2020) 5614, https://doi.org/10.1038/s41598-020-62503-z.
[66] L. Li, M.H. Hubler, Y. Xi, Theoretical modeling on chemical composition and mechanical properties of well cement under carbonation reactions, J. Clean. Prod. 276 (2020) 124270, https://doi.org/10.1016/j.jclepro.2020.124270.
[67] A.E. Morandeau, C.E. White, In situ X-ray pair distribution function analysis of accelerated carbonation of a synthetic calcium–silicate–hydrate gel, J. Mater. Chem. A. 3 (16) (2015) 8597–8605, https://doi.org/10.1039/C5TA00348B.
[68] V. Shah, K. Scrivener, B. Bhattacharjee, S. Bishnoi, Changes in microstructure characteristics of cement paste on carbonation, Cem. Concr. Res. 109 (2018) 184–197, https://doi.org/10.1016/j.cemconres.2018.04.016.
[69] M. Bagheri, S.M. Shariatipour, E. Ganjian, A methodology for reactive transport modelling and geomechanical investigation of wellbores in CO_2 storage sites, Constr. Build. Mater. 268 (2021) 121100, https://doi.org/10.1016/j.conbuildmat.2020.121100.
[70] B.J. Zhan, D.X. Xuan, C.S. Poon, C.J. Shi, S.C. Kou, Characterization of C-S–H formed in coupled CO_2–water cured Portland cement pastes, Mater. Struct. 51 (2018) 92, https://doi.org/10.1617/s11527-018-1211-2.
[71] D. Wang, Y. Fang, Y. Zhang, J. Chang, Changes in mineral composition, growth of calcite crystal, and promotion of physico-chemical properties induced by carbonation of β-C_2S, J. CO_2 Util. 34 (2019) 149–162, https://doi.org/10.1016/j.jcou.2019.06.005.
[72] H. Witkowski, M. Koniorczyk, New sampling method to improve the reliability of FTIR analysis for Self-Compacting Concrete, Constr. Build. Mater. 172 (2018) 196–203, https://doi.org/10.1016/j.conbuildmat.2018.03.216.
[73] O. Omosebi, H. Maheshwari, R. Ahmed, S. Shah, S. Osisanya, A. Santra, A. Saasen, Investigating temperature effect on degradation of well cement in HPHT carbonic acid environment, J. Nat. Gas Sci. Eng. 26 (2015) 1344–1362, https://doi.org/10.1016/j.jngse.2015.08.018.
[74] E.M. Valliant, B.T. Dickey, R. Price, D. Boyd, M.J. Filiaggi, Fourier transform infrared spectroscopy as a tool to study the setting reaction in glass-ionomer cements, Mater. Lett. 185 (2016) 256–259, https://doi.org/10.1016/j.matlet.2016.08.131.
[75] A. Hidalgo, C. Domingo, C. Garcia, S. Petit, C. Andrade, C. Alonso, Microstructural changes induced in Portland cement-based materials due to natural and supercritical carbonation, J. Mater. Sci. 43 (9) (2008) 3101–3111, https://doi.org/10.1007/s10853-008-2521-5.
[76] Z. Tu, C. Shi, N. Farzadnia, Effect of Limestone Powder Content on the Early-Age Properties of CO_2-Cured Concrete, J. Mater. Civ. Eng. 30 (8) (2018) 04018164, https://doi.org/10.1061/(ASCE)MT.1943-5533.0002232.
[77] E.N. Kani, H. Mehdizadeh, Investigating Gel Molecular Structure and Its Relation with Mechanical Strength in Geopolymer Cement Based on Natural Pozzolan Using In Situ ATR-FTIR Spectroscopy, J. Mater. Civ. Eng. 29 (2017) 04017078. doi: 10.1061/(ASCE)MT.1943-5533.0001917.